ROYAL SOCIETY
OF CHEMISTRY

PAPER

Check for updates

Chemical recycling of poly(ethylene terephthalate) *via* sequential glycolysis, oleoyl chloride esterification and vulcanization to yield durable composites†

Claudia V. Lopez and Rhett C. Smith [iD] *

Herein we report a method for the chemical recycling of poly(ethylene terephthalate) (PET) by a three-stage process employing sustainably-sourced organic materials and industrial byproduct sulfur. In this protocol, PET was subject to glycolysis with diethylene glycol to yield low molecular weight oligomers with hydroxyl end groups. The glycolyzed PET (GPET) was then reacted with oleoyl chloride to yield esterified PET (EPET) containing vulcanizable olefin units. The oligomers constituting GPET and EPET were elucidated by MALDI-TOF spectrometry. EPET underwent inverse vulcanization with elemental sulfur (90 wt%) for 35 min or 24 h to yield xPES or mPES, respectively. The composition, thermal, morphological, thermal and mechanical properties were characterized. The composites exhibited good to excellent mechanical properties that were improved significantly by extending the reaction time from 35 min used to prepare xPES (compressive strength = 10.5 MPa, flexural strength = 2.7 MPa) to 24 h used to prepare mPES (compressive strength = 26.9 MPa, flexural strength = 7.7 MPa). Notably, the compressive and flexural strengths of mPES represent 158% and 208% of the values required for residential building foundations made from traditional materials such as ordinary Portland cement. The three-stage approach delineated herein thus represents a way to mediate chemical recycling of waste plastic with green coreagents to yield composites having mechanical properties competitive with existing commercial structural materials.

Introduction

The global production of plastics has increased precipitously over the last half-century.[1] Synthesis of plastic from non-renewable sources like petroleum and natural gas derivatives precludes eternal propagation of this practice. Post-consumer plastics from single-use applications such as food/beverage packaging and diapers, as well as from end-of-use durable goods such as appliances, building materials and furniture persist in the environment to epidemic levels.[2–5] One of the most commonly-used polymers is polyethylene terephthalate (PET). PET is a semi-crystalline polyester produced from the esterification reaction between ethylene glycol and terephthalic acid. Attractive properties of virgin PET such as high tensile and flexural strength and transparency make it one of the most widely used materials in food and beverage packaging and in

the production of synthetic fibres. Of the >100 billion PET bottles produced annually, only ~35 billion are recovered, and as few as ~9 billion of these are ultimately recycled.[1]

Various mechanical and chemical recycling methods have been widely investigated to reclaim PET,[6–11] most commonly through bottle-to-bottle thermal reprocessing or chemical recycling to yield monomers or fuels. Some of the most common chemical recycling routes involve depolymerization of PET by hydrolysis, aminolysis, transesterification, or glycolysis reactions.[12–19] During the glycolysis reaction, for example, PET is depolymerized by heating with glycols such as ethylene glycol or diethylene glycol (Scheme 2), sometimes with the addition of a catalyst, to yield low molecular weight derivatives useful in other processes. The glycolysis reaction of PET with ethylene glycol, for example, can give bis(hydroxyethyl)terephthalate in good yield. This is in turn used in the production of virgin PET.[1]

Esterification reactions are also effective for depolymerizing PET. In one study, new ecological polyester was prepared from PET waste bottles, diethylene glycol and oleic acid.[20] The recycled unsaturated polyester showed enhanced thermal and mechanical properties including an increase of 14.6% in the hardness of the recycled product *versus* PET. This effort to

Department of Chemistry, Clemson University, Clemson, South Carolina, 29634, USA. E-mail: rhett@clemson.edu

† Electronic supplementary information (ESI) available: Additional synthetic and characterization including IR spectra, NMR Spectra, TGA and DSC data, details on mechanical testing. See DOI: https://doi.org/10.1039/d2ma00986b

recycle PET using oleic acid resulted in the formation of a rigid 3-D crosslinked polyester-styrene system. Unsaturated fatty acids and high fatty acid-content fat/oil products having low nutritional value represent an abundant, low-cost feedstock that can be used in reactions that aim to yield value-added products.[21–25]

Ordinary Portland cement (OPC) production accounts for about 30% of global materials utilization with concomitant emission of >8% of anthropogenic CO_2,[26] contributing significantly to increases in global temperatures.[27] Carbon dioxide emission from cement production is only predicted to increase in the next several decades, highlighting the essential but sometimes overlooked role that new structural materials should play in a holistic approach to climate change attenuation.[28] Historically, the monetary cost of cement production was relatively low and the climate cost was not fully understood, so alternatives to OPC were not widely sought outside of some efforts to develop specialty products for applications requiring properties unattainable with OPC. Sulfur cements were one of the few early classes of potential OPC surrogates.[29–34] Such sulfur cements can exhibit high mechanical strength typical of OPC but with greater environmental resilience to acidic conditions and weather-induced degradation.[30–32,35–47]

Most high sulfur content materials (HSMs) reported to date have been prepared by inverse vulcanization (Scheme 1),[48] a reaction analogous to Goodyear's vulcanization,[49] but generally using a greater proportion of sulfur. During inverse vulcanization reactions, sulfur – an underutilized by-product of fossil fuel refining – is heated to temperatures above 159 °C to generate sulfur radicals that react with olefins to generate chemically stable materials with enhanced properties.

Until the green renaissance, sulfur cements were prepared by reacting elemental sulfur with petrochemical olefins. More recently, HSMs have been prepared using a wide range of bioderived comonomers such as polysaccharide derivatives,[50–54] lignin derivatives[55,56] such as guaiacol[57] or chlorolignin,[58] lignocellulosic biomass,[59–61] triglyceride sources,[62] terpenoids,[63,64] and others.[65–68] More recently, novel strategies have been implemented for catalytic inverse vulcanization, mechanochemical synthesis,[69] and lowering reaction temperatures. Concomitant improvements in processing/recycling HSMs have also been developed including use of room-temperature S–S metathesis or combinations of heat/pressure,[1,70–73] Demonstrated application spaces for HSMs[67,74–77] include their use in IR transparent lenses,[78] lithium–sulfur batteries,[79] water purification,[79–96] and in adhesives.[97]

Although numerous bio-olefin-derived HSMs represent promising routes to repurpose biowaste sources into value-added goods, recycled-PET could also be considered a as potential comonomer to be used in the inverse vulcanization process. Such approach could be a valuable addition to current chemical
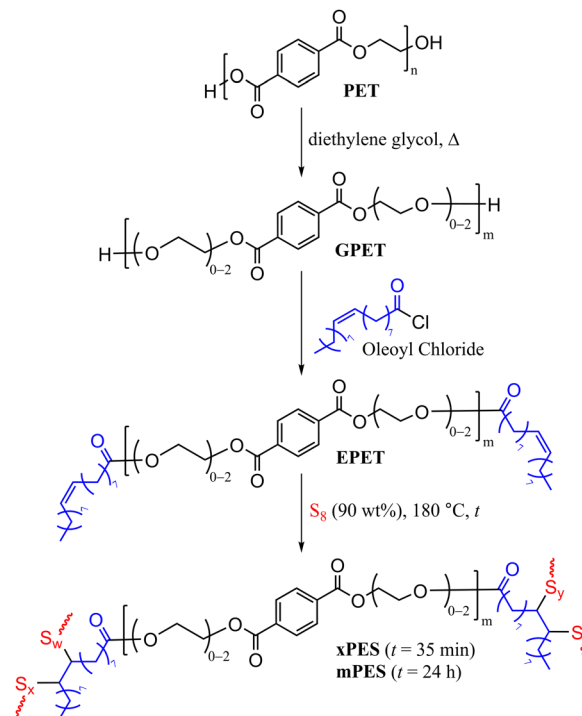
Scheme 2 Sequential glycolysis, esterification, and vulcanization of PET. MALDI-TOF analysis showed that m ranges from 2–6.

recycling strategies to reclaim waste plastic. In the current context, it was thus of interest to (1) depolymerize PET waste using glycols to generate lower molecular weight oligomers. (2) Perform the esterification reaction of the glycolyzed-PET using an unsaturated fatty acid derivative to incorporate olefinic units into the PET polymer chain and (3) Synthesize chemically stable composites with interesting thermal and mechanical properties using the PET-esterified material as the comonomer in the atom economical inverse vulcanization reaction.

Herein, we report the synthesis of HSMs using recycled PET directly as a comonomer in the chemical reaction. This chemical modification was achieved in three steps (Scheme 2): first, the depolymerization of waste PET by diethylene glycol and zinc acetate as the catalyst to yield glycolyzed-PET (GPET). Then GPET reacted with oleoyl to chloride to produce esterified-PET (EPET), and finally, the reaction of 10 wt% EPET with 90 wt% sulfur *via* inverse vulcanization to yield xPES and mPES, where x indicates an "express" synthesis with just 35 min of heating and m indicates more heating over 24 h. The chemical composition, thermal and mechanical properties of the materials will be discussed.

Results and discussion

Depolymerization and esterification of PET

Clear, colourless, postconsumer PET water bottles (M_n = 44 000, M_w = 82 000, PDI = 1.9) were cleaned and cut into small pieces. These PET pieces were rinsed with ethanol and DI water, then dried in a vacuum oven at 40 °C for 24 h. The PET so prepared was subjected to glycolysis by its reaction with diethylene glycol
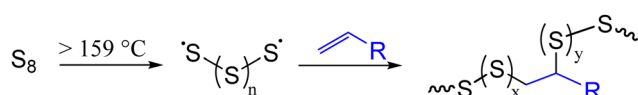
Scheme 1 General inverse vulcanization of an olefin with sulfur.

and zinc acetate for 10 hours at 185 °C according to the reported procedure (Scheme 2, characterization is detailed in the ESI,† Fig. S1–S4 and Table S1),[20] to give GPET. MALDI-TOF spectrometry revealed that GPET is a mixture of oligomers comprising 2–6 terephthalate units (Scheme 2).

Oleoyl chloride was selected as the esterification reagent because it is readily prepared from bio-derived oleic acid and provides the required olefins for crosslinking via vulcanization in the next stage. GPET was therefore reacted with oleoyl chloride under an atmosphere of dry N_2 for 24 h at room temperature to yield the esterified product EPET. EPET was analysed by ^{1}H NMR spectrometry and FT-IR spectroscopy (full spectra along with those of oleoyl chloride for comparison are provided in Fig. S5–S7 in the ESI†). Proton NMR analysis revealed resonances for EPET consistent with the structure shown in Scheme 2. The monomers and oligomers present in EPET were further elucidated by MALDI-TOF spectrometry, which further confirmed the esterification of terminal alcohol moieties in GPET with oleoyl units (MALDI-TOF data and structures of oligomers are provided in Fig. S8 and Table S2 in the ESI†).

The TGA thermogram for EPET (Fig. S4, ESI†) shows a first decomposition step at around 220 °C. This step is attributed to the loss of low molecular fragments via cleavage of ester bonds present between the PET backbone and the oleoyl chloride chain. Similarly, a second degradation step between 360–380 °C represents the cleavage of the polymeric chains in PET.

The total unsaturation content of EPET was quantified by integrating the olefinic proton resonance from oleoyl units (~5.4 ppm) versus the aldehydic proton resonance (~10.2 ppm) of internal standard 2,3,4,5,6-pentafluorobenzaldehyde (full spectrum provided in Fig. S6 in the ESI†). This analysis revealed that EPET has 3.6 mmol g^{-1} of olefin moieties that could undergo a vulcanization reaction.

Synthesis and chemical characterization of composites

In the third step of the process shown in Scheme 2, the reaction of 90 wt% sulfur and 10 wt% EPET at 185 °C was undertaken. Prior work has noted that monomer composition, heating time and conditions can significantly impact the properties of HSMs prepared by inverse vulcanization.[98] To explore the limits of reaction time influence, the vulcanization of EPET was undertaken under identical conditions for either 35 min to yield xPES, or 24 h to yield mPES. After the designated heating time, each reaction mixture was cooled to room temperature, giving a quantitative yield of either xPES as a light-brown solid or mPES as a black solid (Fig. 1). Both the composites are remeltable solids, allowing them to be readily poured into moulds in the heated liquid form and then cooled to give samples shapes such as cylinders (Fig. 1(A) and (C)) or dog-bones (Fig. 1(B) and (D)) appropriate for compressive strength or tensile strength testing, respectively. Previous work has demonstrated a correlation between sulfur catenate length (and thus crosslink density or sulfur rank) and the colour of the material, with a lighter colour generally indicative of shorter catenates.[99,100] The less-crosslinked
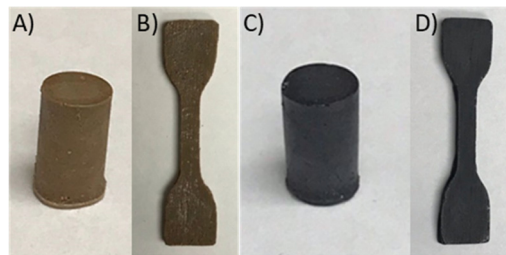

Fig. 1 Samples of xPES (A), (B) and mPES (C), (D) shaped for compressive (A) and (C) or tensile (B) and (D) strength testing.

nature of light brown-coloured xPES was supported by fractionation studies and mechanical tests (vide infra).

The FT-IR spectra for xPES and mPES (Fig. S9, ESI†) confirm the loss of intensity for bands attributable to sp^2 C–H stretches for cis-alkenes that had been present in EPET at around 3005 cm^{-1} with concomitant emergence of a peak at 664 cm^{-1} attributed to C–S stretches from the bonds formed during the inverse vulcanization process.

Notably, the inverse vulcanization process is 100% atom economical in this case. In some inverse vulcanization reactions, the atom economy falls below 100% due to H_2S formation, typically via sulfur radical-mediated abstraction of benzylic or allylic protons or loss of sublimed sulfur. In the current case the vessel was covered with a watch glass to preclude sublimation loss and no side reaction-derived mass loss was observable: a 100% yield of the target composites was accomplished within the error limits of mass measurement.

HSMs prepared by inverse vulcanization are generally best described as composites because there is a small percentage of added sulfur that is not covalently incorporated into the organic-sulfur network. Several techniques have been reported to quantify the free versus bound sulfur in HSMs.[101] Free sulfur (S_8) is completely soluble in CS_2, while sulfur that is covalently crosslinked in a densely-crosslinked sulfur/olefin network is not soluble in CS_2. This solubility difference allowed us to use fractionation studies using CS_2 to quantify free versus covalently incorporated sulfur in xPES and mPES composites. In the current study, CS_2 extractions followed by elemental analysis of the fractions revealed that most of the sulfur present in the composites was effectively incorporated as covalently-bound catenates as indicated in Scheme 1. Composite xPES had only 10 wt% of extractable free sulfur, while mPES had 20 wt% of CS_2-extractable material. The heating time had a notable impact on the chemical composition of the extractable portions of the composites. Elemental microanalysis of the CS_2-extractable fraction of mPES was found to be 98% elemental sulfur, indicating that essentially all of the organic molecules from EPET have been effectively sequestered into the insoluble network solid through the formation of C–S bonds over 24 h of heating in the vulcanization reaction. In sharp contrast, the soluble fraction of xPES was 93% sulfur, with 7% of the mass attributable to extractable organic material (Table S2, ESI†). These data suggest that lower molecular-mass fragments not comprising part of the network solid are still present after the

abbreviated 35 min heating time. These data, and the mechanical properties of the composites (*vide infra*) reinforce the sensitive nature of HSMs to heating time. Given that essentially all of the organic comonomer comprises part of the network polymer in mPES and the amount of sulfur effectively incorporated into the network is also known, the average length of the oligosulfur catenates linking organic units (known as a material's sulfur rank) was calculated (details are in the ESI†). A wide range of average sulfur ranks, from 1 to >500, have been reported for other vulcanized materials depending on the olefin content and the proportion of sulfur employed for their synthesis. For mPES the sulfur rank was thus found to be 62. This compares well to other composites prepared by inverse vulcanization with 90 wt% sulfur, such as CanBG$_{90}$[25] and OSS$_{90}$,[53] which have similar sulfur ranks to that in mPES, of 60 and 69, respectively. The organic crosslinker for CanBG$_{90}$ was 1:1 (mass/mass) brown grease (a high fatty acid-content animal fat) and sunflower oil, while for OSS$_{90}$ the organic crosslinker was octenyl succinate-modified cellulose.

Thermal, morphological and mechanical properties of composites

TGA of composites xPES and mPES (Fig. S4, ESI†) revealed decomposition temperatures (T_d) of 217 °C and 215 °C, respectively (Table 1). These T_d values lie within the range of other composites comprising similarly high proportions of sulfur, wherein thermally-induced mass loss is attributable to degradation of the polysulfide domains.

Differential scanning calorimetry (DSC, Table 1 and Fig. S10 of the ESI†) was used to investigate the composites' thermal/morphological transitions over the range of −60 to 140 °C. Both xPES and mPES exhibited the characteristic melting peak of orthorhombic sulfur at temperatures between 115 and 118 °C. In the second heating cycle, xPES and mPES showed glass transitions (T_g) at −37 °C, diagnostic for the presence of polymeric sulfur catenates in the organosulfur crosslinked network. Cold crystallization peaks were also observed in xPES and mPES at 15 and 3.7 °C, respectively. These cold crystallization peaks reflect the partial organization of the polymer chains above the glass transition temperature, which is commonly observed in network-stabilized polymeric sulfur domains.

The percent crystallinity of xPES and mPES relative to crystalline orthorhombic sulfur was calculated from the integration of melting and cold crystallization enthalpies observed

in the DSC spectra (the equation used for the calculations is provided in the Experimental section). From these integrations, it can be concluded that both composites have amorphous and crystalline regions, with percent crystallinities between 25–34% (Table 1).

Scanning electron microscopy with elemental mapping by energy-dispersive X-ray analysis (SEM-EDX) confirmed that xPES and mPES form microscopically homogeneous materials (Fig. S13 in ESI†). In both cases, the composites had largely uniform distributions of carbon, oxygen and sulfur. These data provide further evidence of the successful chemical reaction between EPET and elemental sulfur to yield homogeneous composites.

Cylinders, dog-bones, and rectangular prisms of the composites for compressive, tensile, and flexural strength testing, respectively, were readily prepared by melting the xPES and mPES composites at 160 °C and pouring the liquid into silicon moulds (examples are shown in Fig. 1). The composites were allowed to stand at room temperature for four days before any mechanical testing to allow direct compare their mechanical properties to those of reported HSMs that are likewise aged for four days prior to measurement.[25,62,63]

Mechanical test stand analysis was used to measure the compressive strength of composites (Fig. 2(A) and Table 2; stress–strain plots are provided in Fig. S11 in the ESI†). The compressive strength of xPES was 10.5 ± 0.1 MPa, representing 62% of the compressive strength of ordinary Portland cement (OPC). The compressive strength of mPES, however, was 26.9 ± 0.6 MPa, which is 158% of the compressive strength of OPC. The significantly lower compressive strength of xPES *versus* that of mPES may be attributed to a lower extent of crosslinking in xPES as a result of the shorter reaction time. This hypothesis is supported by incomplete incorporation of organics into the network structure that was observed in fractionation studies (*vide supra*, Table S1 in ESI†). Composites comprise vulcanized aromatic/fatty acid components, so a comparison of their properties to those of other vulcanized composites comprising fatty acid or aromatic subunits with 90 wt% sulfur is also of interest. Composite mPES, for example exhibits a lower compressive strength than that of CanBG$_{90}$,[25] which has significant fatty acid and triglyceride content but no aromatic moieties. On the other hand, the compressive strength of mPES is significantly higher than that of ZOS$_{90}$ (19.4 MPa) that employed oleic acid as the organic comonomer, or PS$_{90}$ (21.3 MPa)[59,60]

Table 1 Thermal and morphological properties with comparison to elemental sulfur

Materials	$T_d{}^a$/°C	$T_m{}^b$/°C	$T_{g,DSC}{}^c$/°C	Cold crystallization peaks/°C	ΔH_m J g^{-1}	ΔH_{cc} J g^{-1}	Percent crystallinity^d	Percent insoluble fraction^e
xPES	217	117.7	−36.8	15.0	33.9	−22.8	25	90
mPES	215	116.8	−36.0	3.7	33.6	−18.2	34	80
GPET	176	NA	NA	NA	NA	NA	NA	NA
EPET	221	NA	NA	NA	NA	NA	NA	NA
S$_8$	229	118.5	NA	NA^b	44.8	NA	100	0

^{a} The temperature at which the 5% mass loss was observed. ^{b} The temperature at the peak maximum of the endothermic melting from the third heating cycle. ^{c} Glass transition temperature. ^{d} The reduction of percent crystallinity of each sample was calculated with respect to sulfur (normalized to 100%). ^{e} Percent of non-extractable sulfur in each sample after CS$_2$ extractions.
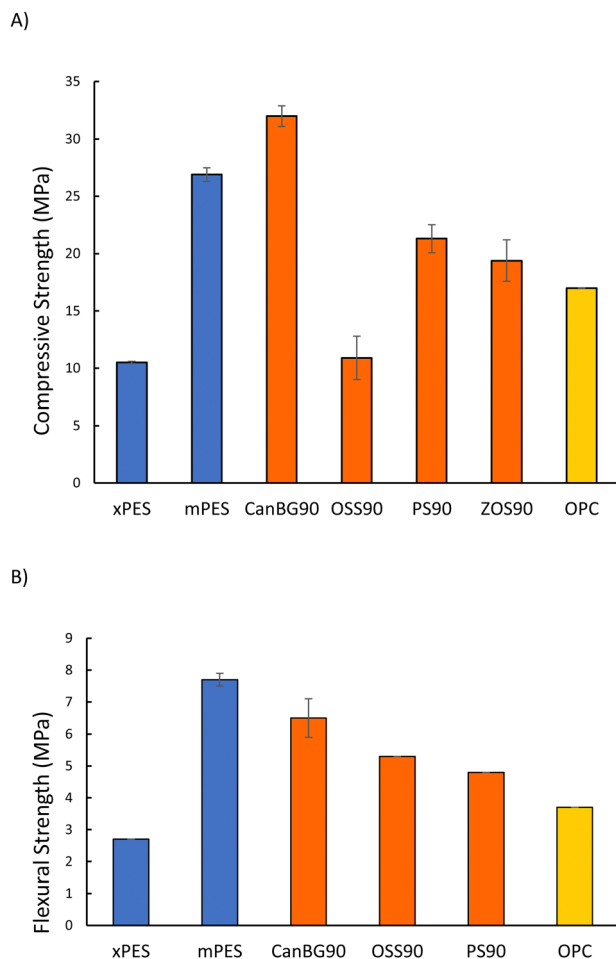
A)

B)

Fig. 2 Compressive strength (A) and flexural strength (B) for composites xPES and,PES compared to other high sulfur-content materials and the familiar structural product ordinary Portland cement (OPC).

containing lignocellulosic biomass (peanut shells having only ~1 wt% triglyceride content).

PES composites were also subjected to dynamic mechanical analysis (DMA) at room temperature in single cantilever mode to assess their flexural strengths/moduli (Fig. 2(B) and Table 2; stress–strain plots are provided in Fig. S12 in the ESI†). As with the compressive tests, mPES exhibited significantly higher flexural strength and moduli than that of xPES. The flexural

strength of mPES is higher than those reported for CanBG$_{90}$ (6.5 MPa), PS$_{90}$ (4.8 MPa), or OSS$_{90}$ (5.3 MPa).

The ultimate tensile strength at break (UTS) of mPES (0.21 MPa), was similar to that of xPES (0.27 MPa), with both materials showing relatively poor tensile performance and low elongation at break (<1%) as compared to previously reported composites having similar sulfur content and aromatic organic crosslinking groups. Composites GS$_{80}$ (UTS = 2.32 MPa, elongation at break = 4%) and GS$_{90}$ (UTS = 1.16 MPa, elongation at break = 11%), for example, were prepared by crosslinking guaiacol and 80 or 90 wt% sulfur, respectively.[57] Composite I-BPA$_{80}$, prepared by inverse vulcanization of (O,O'-diallyl-2,2',6,6'-tetrabromo bisphenol A and 80 wt% sulfur) exhibited a similar UTS (1.04 MPa) to GS$_{90}$ with a significantly greater elongation at break of 89 ± 9%.[70]

Conclusions

The chemical recycling of poly(ethylene terephthalate) was achieved in a process that involved the glycolysis of waste PET by diethylene glycol followed by its esterification reaction using fatty acid derivatives to yield esterified-PET (EPET). EPET was then directly used as the organic comonomer in the inverse vulcanization reaction with elemental sulfur and a variation in the reaction time (35 min or 24 h) yielded composites xPES and mPES, respectively. The influence of extending the reaction times in the chemical and mechanical properties of the composites was evaluated. The longer reaction time led to significantly higher compressive and flexural strength for mPES than for xPES. This improvement in the mechanical properties of mPES can be attributed to a more complete crosslinking of the organic domains in the composite after 24 h of reaction, as confirmed by fractionation studies. The synthetic approach to repurposing PET reported herein represents a promising way to directly incorporate waste PET as the organic comonomer in the atom economical inverse vulcanization reaction to yield sustainable building materials with mechanical properties that exceed that of commercial structural materials.

Experimental

General considerations and instrumentation

Matrix assisted laser desorption/ionization time of flight mass spectrometry (MALDI-TOF) data were recorded on a MicrofleX

Table 2   Physical properties of composites compared to other previously-reported high sulfur content materials

Materials	Compressive strength (MPa)	Flexural strength/modulus (MPa)	Ultimate tensile strength at break (MPa)	Elongation at break (%)	Sulfur rank	Ref.
xPES	10.5 ± 0.1	2.7/100	0.27 ± 0.02	<1	ND	This work
mPES	26.9 ± 0.6	7.7/320	0.21 ± 0.04	<1	62	This work
CanBG$_{90}$	32.0 ± 0.9	6.5/420	ND	ND	60	23
OSS$_{90}$	10.9 ± 1.9	5.3/660	ND	ND	69	51
PS$_{90}$	21.3 ± 1.2	4.8/950	ND	ND	257	57,58
ZOS$_{90}$	19.4 ± 1.8	ND	ND	ND	ND	22
GS$_{80}$	ND	ND	2.32 ± 0.02	10.9 ± 2.1	ND	55
GS$_{90}$	ND	ND	1.16 ± 0.53	4.3 ± 1.8	ND	55
I-BPA$_{80}$	ND	ND	1.04 ± 0.16	89 ± 9	ND	68
Portland cement	17.0	3.7/580	ND	ND	NA	—

LRF equipped with a 337 nm nitrogen laser in the positive reflectron ion mode. The scanning mass-to-charge (m/z) range for the experiments was between 600–1600 using α-cyano-4-hydroxycinnamic acid as the matrix.

Fourier transform infrared spectra were obtained using an IR instrument (Shimadzu IRAffinity-1S) with an ATR (attenuated total reflectance) attachment. Scans were collected over the range 400–4000 cm^{-1} at ambient temperature with a resolution of 8.

SEM was acquired on a Schottky Field Emission Scanning Electron Microscope SU5000 operating in variable pressure mode with an accelerating voltage of 15 keV.

TGA data were recorded using a Mettler Toledo TGA 2 STAR^e System operating over the range 20–800 °C with a heating rate of 10 °C min^{-1} under a flow of N$_2$ (100 mL min^{-1}). Each measurement was acquired in triplicate and presented results represent an average value.

DSC data were acquired using a Mettler Toledo DSC 3 STAR^e System operating over the range −60 to 140 °C with a heating rate of 10 °C min^{-1} under a flow of N$_2$ (200 mL min^{-1}). Each DSC measurement was carried out over three heat–cool cycles.

DMA was performed using a Mettler Toledo DMA 1 STAR^e System in single cantilever mode. DMA samples were cast from silicone resin moulds made using a commercial Smooth-On Oomoo® 30 tin-cure kit. Samples were manually sanded to ensure uniform dimensions of approximately $15 \times 8 \times 1.5$ mm. Sample dimensions were measured using a digital calliper with 0.01 mm resolution. The force was varied from 0 to 10 N with a ramp rate of 0.2 N min^{-1} measured isothermally at 25 °C.

Carbon disulfide extractions were performed by suspending 0.3 g of finely ground material (measured to 0.0001 g accuracy) in 20 mL of CS$_2$, allowing the solid to settle for 30 minutes, pipetting off the supernatant into a separate vial, and adding another 20 mL of CS$_2$. This process was repeated an additional three times so that a total of 5 washes were performed and constant residual mass was confirmed. The residual CS$_2$ was evaporated under a flow of N$_2$, and each vial was weighed to determine the fraction that was soluble (collected as supernatant) or insoluble (remained in the initial vial). This process was performed in duplicate, yielding identical results within balance error both times for each material analysed.

Compressional analysis was performed on a Mark-10 ES30 test stand equipped with an M3-200 force gauge (1 kN maximum force with 1 N resolution) with an applied force rate of 3–4 N s^{-1}. Compression cylinders were cast from silicone resin moulds (Smooth-On Oomoo 30 tin-cure) with diameters of approximately 6 mm and heights of approximately 10 mm. Samples were manually sanded to ensure uniform dimensions and measured with a digital calliper with 0.01 mm resolution. Compressional analysis was performed in triplicate and results were averaged.

Proton NMR spectra were acquired on a Bruker NEO-300 MHz at room temperature and data was processed with TopSpin 4.0.6 software. All spectra reported were calibrated to the residual solvent signal.

Materials

Diethylene glycol (VWR), zinc acetate (Sigma Aldrich), oleoyl chloride (Sigma Aldrich), and sulfur (Dugas Diesel) were used without further purification. PET-sulfur composite materials were aged for 4 d prior to any mechanical testing.

Synthesis

CAUTION: Heating elemental sulfur with organics can result in the formation of H$_2$S gas. H$_2$S is toxic, foul-smelling, and corrosive. Although we did not observe any mass loss attributable to gas generation, the temperature must be carefully controlled to prevent thermal spikes, which contribute to the potential for H$_2$S evolution. Rapid stirring shortened heating times, and very slow addition of reagents can help prevent unforeseen temperature spikes.

Synthesis of xPES

Preparation of xPES involved the reaction of EPET (1.0 g, 10 wt%) and sulfur (9.0 g, 0.03 mol, 90 wt%). Sulfur was first melted in an oil bath at 160 °C with rapid mechanical stirring. Then, the temperature was heated further to 185 °C, where sulfur exists primarily as polymeric diradicals. Once the temperature was stable, EPET was slowly added to the sulfur while stirring. The reaction mixture was stirred for 35 min at 185 °C. Within 35 min of the reaction time, the desired product, a homogeneous solution was produced. Upon cooling to room temperature, the material solidified to a light-brown solid composite in quantitative yield (10 g). ELEM. ANAL calcd: C 4.00, H 1.00, S 90.00; found: C 7.61, H 1.11, S 89.28.

Synthesis of mPES

Preparation of mPES involved the reaction of EPET (1.0 g, 10 wt%) and sulfur (9.0 g, 0.03 mol, 90 wt%). Sulfur was first melted in an oil bath at 160 °C with rapid mechanical stirring. Then, the temperature was heated further to 185 °C, where sulfur exists primarily as polymeric diradicals. Once the temperature was stable, EPET was slowly added to the sulfur while stirring. The reaction mixture was stirred for 24 h at 185 °C. Within 24 h of the reaction time, the desired product, a homogeneous solution was produced. Upon cooling to room temperature, the material solidified to a black solid composite in quantitative yield (10 g). ELEM. ANAL calcd: C 4.00, H 1.00, S 90.00; found: C 8.22, H 0.50, S 90.48.

Author contributions

Claudia Lopez: data curation, formal analysis, investigation, validation, roles/writing – original draft. Rhett C. Smith: conceptualization, funding acquisition, methodology, resources, supervision, writing – review and editing.

Conflicts of interest

There are no conflicts to declare.

Acknowledgements

Notes and references

1 T. Thiounn and R. C. Smith, *J. Polym. Sci.*, 2020, **58**, 1347–1364.

2 J. Jeong and J. Choi, *Chemosphere*, 2019, **231**, 249–255.

3 M. Cole, P. Lindeque, C. Halsband and T. S. Galloway, *Mar. Pollut. Bull.*, 2011, **62**, 2588–2597.

4 V. Hidalgo-Ruz, L. Gutow, R. C. Thompson and M. Thiel, *Environ. Sci. Technol.*, 2012, **46**, 3060–3075.

5 I. Gestoso, E. Cacabelos, P. Ramalhosa and J. Canning-Clode, *Sci. Total Environ*, 2019, **687**, 413–415.

6 B. S. Maddodi, L. U. A, S. Devesh, A. U. Rao, G. B. Shenoy, H. T. Wijerathne, N. Sooriyaperkasam and P. K. M, *Eng. Sci.*, 2022, **18**, 329–336.

7 D. Pan, F. Su, H. Liu, C. Liu, A. Umar, L. C. Castañeda, H. Algadi, C. Wang and Z. Guo, *ES Mater. Manuf.*, 2021, **11**, 3–15.

8 N. George and T. Kurian, *Ind. Eng. Chem. Res.*, 2014, **53**, 14185–14198.

9 K. M. Akato, N. A. Nguyen, P. V. Bonnesen, D. P. Harper and A. K. Naskar, *ACS Omega*, 2018, **3**, 10709–10715.

10 B. Geyer, G. Lorenz and A. Kandelbauer, *eXPRESS Polym. Lett.*, 2016, **10**, 559–586.

11 A. M. Al-Sabagh, F. Z. Yehia, G. Eshaq, A. M. Rabie and A. E. ElMetwally, *Egypt. J. Pet.*, 2016, **25**, 53–64.

12 E. Langer, S. Waśkiewicz, M. Lenartowicz-Klik and K. Bortel, *Polym. Degrad. Stab.*, 2015, **119**, 105–112.

13 D. J. Suh, O. O. Park and K. H. Yoon, *Polymer*, 2000, **41**, 461–466.

14 B. Liu, X. Lu, Z. Ju, P. Sun, J. Xin, X. Yao, Q. Zhou and S. Zhang, *Ind. Eng. Chem. Res.*, 2018, **57**, 16239–16245.

15 K. Troev, G. Grancharov, R. Tsevi and I. Gitsov, *J. Appl. Polym. Sci.*, 2003, **90**, 1148–1152.

16 Q. Wang, Y. Geng, X. Lu and S. Zhang, *ACS Sustainable Chem. Eng.*, 2015, **3**, 340–348.

17 H. Wang, Z. Li, Y. Liu, X. Zhang and S. Zhang, *Green Chem.*, 2009, **11**, 1568–1575.

18 Q. F. Yue, C. X. Wang, L. N. Zhang, Y. Ni and Y. X. Jin, *Polym. Degrad. Stab.*, 2011, **96**, 399–403.

19 O. Mecit and A. Akar, *Macromol. Mater. Eng.*, 2001, **286**, 513–515.

20 H. M. Naguib and X. H. Zhang, *Polym. Test.*, 2018, **69**, 450–455.

21 A. D. Smith, T. Thiounn, E. W. Lyles, E. K. Kibler, R. C. Smith and A. G. Tennyson, *J. Polym. Sci., Part A: Polym. Chem.*, 2019, **57**, 1704–1710.

22 A. D. Smith, C. D. McMillen, R. C. Smith and A. G. Tennyson, *J. Polym. Sci.*, 2020, **58**, 438–445.

23 A. D. Smith, C. D. McMillin, R. C. Smith and A. G. Tennyson, *J. Polym. Sci.*, 2020, **58**, 438–445.

24 A. D. Smith, R. C. Smith and A. G. Tennyson, *Sustainable Chem. Pharm.*, 2020, **16**, 100249.

25 C. V. Lopez, A. D. Smith and R. C. Smith, *RSC Adv.*, 2022, **12**, 1535–1542.

26 K. L. Scrivener, V. M. John and E. M. Gartner, *Cem. Concr. Res.*, 2018, **114**, 2–26.

27 P. A. Arias, N. Bellouin, E. Coppola, R. G. Jones, G. Krinner, J. Marotzke, V. Naik, M. D. Palmer, G.-K. Plattner, J. Rogelj, M. Rojas, J. Sillmann, T. Storelvmo, P. W. Thorne, B. Trewin, K. A. Rao, B. Adhikary, R. P. Allan, K. Armour, G. Bala, R. Barimalala, S. Berger, J. G. Canadell, C. Cassou, A. Cherchi, W. Collins, W. D. Collins, S. L. Connors, S. Corti, F. Cruz, F. J. Dentener, C. Dereczynski, A. D. Luca, A. D. Niang, F. J. Doblas-Reyes, A. Dosio, H. Douville, F. Engelbrecht, V. Eyring, E. Fischer, P. Forster, B. Fox-Kemper, J. S. Fuglestvedt, J. C. Fyfe, N. P. Gillett, L. Goldfarb, I. Gorodetskaya, J. M. Gutierrez, R. Hamdi, E. Hawkins, H. T. Hewitt, P. Hope, A. S. Islam, C. Jones, D. S. Kaufman, R. E. Kopp, Y. Kosaka, J. Kossin, S. Krakovska, J.-Y. Lee, T. M. J. Li, T. K. Maycock, M. Meinshausen, S.-K. Min, P. M. S. Monteiro, T. Ngo-Duc, F. Otto, I. Pinto, A. Pirani, K. Raghavan, R. Ranasinghe, A. C. Ruane, L. Ruiz, J.-B. Sallée, B. H. Samset, S. Sathyendranath, S. I. Seneviratne, A. A. Sörensson, S. Szopa, I. Takayabu, A.-M. Treguier, B. V. D. Hurk, R. Vautard, K. V. Schuckmann, S. Zaehle, X. Zhang and K. Zickfeld, in *Climate Change 2021: The Physical Science Basis. Contribution of Working Group I to the Sixth Assessment Report of the Intergovernmental Panel on Climate Change*, ed. V. Masson-Delmotte, P. Zhai, A. Pirani, S. L. Connors, C. Péan, S. Berger, N. Caud, Y. Chen, L. Goldfarb, M. I. Gomis, M. Huang, K. Leitzell, E. Lonnoy, J. B. R. Matthews, T. K. Maycock, T. Waterfield, O. Yelekçi, R. Yu and B. Zhou, Cambridge University Press, 2021.

28 R. M. Andrew, *Earth Syst. Sci. Data*, 2018, **10**, 195–217.

29 A.-M. O. Mohamed and M. E. Gamal, *Sulfur concrete for the construction industry*, J. Ross Publishing, Fort Lauderdale, FL, 2010.

30 Journal, 1978.

31 M. Al-Ansary, E. Masad and D. Strickland, *Adv. Gas Process.*, 2010, **2**, 121–130.

32 A. Taylor, N. Tran, R. May, D. Timm, M. Robbins and B. Powell, *J. Assoc. Asphalt Paving Technol.*, 2010, **79**, 403–441.

33 Z.-g Zuo, G.-s Cao and H.-l Song, *J. Qingdao Technol. Univ.*, 2011, **32**, 26–29.

34 X.-D. Hu, Y.-M. Gao, L.-R. Lin, S. Zhong and X.-W. Dai, *J. Wuhan Univ. Technol.*, 2013, **35**, 10–13.

35 M. Dehestani, E. Teimortashlu, M. Molaei, M. Ghomian, S. Firoozi and S. Aghili, *Data Brief*, 2017, **13**, 137–144.

36 E. D. Weil, *Phosphorus, Sulfur Silicon Relat. Elem.*, 1991, **59**, 325–340.

37 WO2004-EP53357, 2005.

38 I. Deme, *Adv. Chem. Ser.*, 1978, **165**, 172–189.

39 J. E. Gillott, I. J. Jordaan, R. E. Loov, N. G. Shrive and M. A. Ward, *Adv. Chem. Ser.*, 1978, **165**, 98–112.

40 G. J. Kennepohl and L. J. Miller, *Adv. Chem. Ser.*, 1978, **165**, 113–134.

41 D.-Y. Lee, *Prod. R&D*, 1975, **14**, 171–177.

42 S. Gwon, E. Ahn and M. Shin, *Composites, Part B*, 2019, **162**, 469–483.

43 S. Gwon, S.-Y. Oh and M. Shin, *Constr. Build. Mater.*, 2018, **181**, 276–286.

44 S. Gwon and M. Shin, *Constr. Build. Mater.*, 2019, **228**, 116784.

45 P. Szajerski, A. Bogobowicz and A. Gasiorowski, *J. Hazard. Mater.*, 2020, **381**, 121180.

46 M. Lewandowski and R. Kotynia, *MATEC Web Conf.*, 2018, **219**, 3006.

47 S. Mohammed and V. Poornima, *Mater. Today: Proc.*, 2018, **5**, 23888–23897.

48 W. J. Chung, J. J. Griebel, E. T. Kim, H. Yoon, A. G. Simmonds, H. J. Ji, P. T. Dirlam, R. S. Glass, J. J. Wie, N. A. Nguyen, B. W. Guralnick, J. Park, A. Somogyi, P. Theato, M. E. Mackay, Y.-E. Sung, K. Char and J. Pyun, *Nat. Chem.*, 2013, **5**, 518–524.

49 US3633A, *Goodyear Charles*, 1844.

50 M. K. Lauer, T. A. Estrada-Mendoza, C. D. McMillen, G. Chumanov, A. G. Tennyson and R. C. Smith, *Adv. Sustainable Syst.*, 2019, **3**, 1900062.

51 M. K. Lauer and R. C. Smith, *Compr. Rev. Food Sci. Food Saf.*, 2020, **19**, 1–53, DOI: 10.1111/1541-4337.12627.

52 M. K. Lauer, A. G. Tennyson and R. C. Smith, *ACS Appl. Polym. Mater.*, 2020, **2**, 3761–3765.

53 M. K. Lauer, A. G. Tennyson and R. C. Smith, *Mater. Adv.*, 2021, **2**, 2391–2397.

54 M. K. Lauer, A. G. Tennyson and R. C. Smith, *Mater. Adv.*, 2022, **3**, 4186–4193.

55 M. S. Karunarathna, M. K. Lauer, T. Thiounn, R. C. Smith and A. G. Tennyson, *J. Mater. Chem. A*, 2019, **7**, 15683–15690.

56 M. S. Karunarathna and R. C. Smith, *Sustainability*, 2020, **12**, 734–748.

57 M. S. Karunarathna, M. K. Lauer and R. C. Smith, *J. Mater. Chem. A*, 2020, **8**, 20318–20322.

58 M. S. Karunarathna, A. G. Tennyson and R. C. Smith, *J. Mater. Chem. A*, 2020, **8**, 548–553.

59 M. K. Lauer, M. S. Karunarathna, A. G. Tennyson and R. C. Smith, *Mater. Adv.*, 2020, **1**, 590–594.

60 M. K. Lauer, M. S. Karunarathna, A. G. Tennyson and R. C. Smith, *Mater. Adv.*, 2020, **1**, 2271–2278.

61 M. K. Lauer, Z. E. Sanders, A. D. Smith and R. C. Smith, *Mater. Adv.*, 2021, **2**, 7413–7422.

62 C. V. Lopez, M. S. Karunarathna, M. K. Lauer, C. P. Maladeniya, T. Thiounn, E. D. Ackley and R. C. Smith, *J. Polym. Sci.*, 2020, **58**, 2259–2266.

63 C. P. Maladeniya, M. S. Karunarathna, M. K. Lauer, C. V. Lopez, T. Thiounn and R. C. Smith, *Mater. Adv.*, 2020, **1**, 1665–1674.

64 C. P. Maladeniya and R. C. Smith, *J. Compos. Sci.*, 2021, **5**, 257.

65 M. S. Karunarathna, M. K. Lauer, A. G. Tennyson and R. C. Smith, *Polym. Chem.*, 2020, **11**, 1621–1628.

66 T. Thiounn, M. K. Lauer, M. S. Karunarathna, A. G. Tennyson and R. C. Smith, *Sustainable Chem.*, 2020, **1**, 183–197.

67 T. Thiounn, M. K. Lauer, M. S. Bedford, R. C. Smith and A. G. Tennyson, *RSC Adv*, 2018, **8**, 39074–39082.

68 T. Thiounn, A. G. Tennyson and R. C. Smith, *RSC Adv.*, 2019, **9**, 31460–31465.

69 P. Yan, W. Zhao, F. McBride, D. Cai, J. Dale, V. Hanna and T. Hasell, *Nat. Commun.*, 2022, **13**, 4824.

70 T. Thiounn, M. S. Karunarathna, L. M. Slann, M. K. Lauer and R. C. Smith, *J. Polym. Sci.*, 2020, **58**, 2943–2950.

71 S. J. Tonkin, C. T. Gibson, J. A. Campbell, D. A. Lewis, A. Karton, T. Hasell and J. M. Chalker, *Chem. Sci.*, 2020, **11**, 5537–5546.

72 N. A. Lundquist, A. D. Tikoalu, M. J. H. Worthington, R. Shapter, S. J. Tonkin, F. Stojcevski, M. Mann, C. T. Gibson, J. R. Gascooke, A. Karton, L. C. Henderson, L. J. Esdaile and J. M. Chalker, *Chem. – Eur. J.*, 2020, **26**, 10035–10044.

73 K. Orme, A. H. Fistrovich and C. L. Jenkins, *Macromolecules*, 2020, **53**, 9353–9361.

74 B. Zhang, H. Gao, P. Yan, S. Petcher and T. Hasell, *Mater. Chem. Front.*, 2020, **4**, 669–675.

75 P. Yan, W. Zhao, B. Zhang, L. Jiang, S. Petcher, J. A. Smith, D. J. Parker, A. I. Cooper, J. Lei and T. Hasell, *Angew. Chem., Int. Ed.*, 2020, **59**, 13371–13378.

76 C. R. Westerman and C. L. Jenkins, *Macromolecules*, 2018, **51**, 7233–7238.

77 C. R. Westerman, P. M. Walker and C. L. Jenkins, *J. Visualized Exp.*, 2019, e59620, DOI: 10.3791/59620.

78 J. J. Griebel, S. Namnabat, E. T. Kim, R. Himmelhuber, D. H. Moronta, W. J. Chung, A. G. Simmonds, K.-J. Kim, J. van der Laan, N. A. Nguyen, E. L. Dereniak, M. E. MacKay, K. Char, R. S. Glass, R. A. Norwood and J. Pyun, *Adv. Mater.*, 2014, **26**, 3014–3018.

79 C. V. Lopez, C. P. Maladeniya and R. C. Smith, *Electrochem.*, 2020, **1**, 226–259.

80 M. L. Eder, C. B. Call and C. L. Jenkins, *ACS Appl. Polym. Mater.*, 2022, **4**, 1110–1116.

81 J. H. Worthington Max, L. Kucera Renata, T. Gibson Christopher, A. Sibley, D. Slattery Ashley, A. Campbell Jonathan, F. K. Alboaiji Salah, J. Young, N. Adamson, R. Gascooke Jason, A. Lewis David, S. Quinton Jamie, V. Ellis Amanda, M. Chalker Justin, S. Albuquerque Ines, J. L. Bernardes Goncalo, A. Muller Katherine, A. Johs, D. Jampaiah, M. Sabri Ylias, K. Bhargava Suresh and J. Ippolito Samuel, *Chemistry*, 2017, **23**, 16219–16230.

82 L. J. Esdaile and J. M. Chalker, *Chemistry*, 2018, **24**, 6905–6916.

83 M. J. H. Worthington, C. J. Shearer, L. J. Esdaile, J. A. Campbell, C. T. Gibson, S. K. Legg, Y. Yin, N. A. Lundquist, J. R. Gascooke, I. S. Albuquerque, J. G. Shapter, G. G. Andersson, D. A. Lewis, G. J. L. Bernardes and J. M. Chalker, *Adv. Sustainable Syst.*, 2018, **2**, 1800024.

84 Y. Zhang, T. S. Kleine, K. J. Carothers, D. D. Phan, R. S. Glass, M. E. MacKay, K. Char and J. Pyun, *Polym. Chem.*, 2018, **9**, 2290–2294.

85 Y. Zhang, J. J. Griebel, P. T. Dirlam, N. A. Nguyen, R. S. Glass, M. E. MacKay, K. Char and J. Pyun, *J. Polym. Sci., Part A: Polym. Chem.*, 2017, **55**, 107–116.
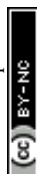
86 P. T. Dirlam, R. S. Glass, K. Char and J. Pyun, *J. Polym. Sci., Part A: Polym. Chem.*, 2017, **55**, 1635–1668.

87 T. S. Kleine, N. A. Nguyen, L. E. Anderson, S. Namnabat, E. A. LaVilla, S. A. Showghi, P. T. Dirlam, C. B. Arrington, M. S. Manchester, J. Schwiegerling, R. S. Glass, K. Char, R. A. Norwood, M. E. Mackay and J. Pyun, *ACS Macro Lett.*, 2016, **5**, 1152–1156.

88 P. T. Dirlam, A. G. Simmonds, T. S. Kleine, N. A. Nguyen, L. E. Anderson, A. O. Klever, A. Florian, P. J. Costanzo, P. Theato, M. E. Mackay, R. S. Glass, K. Char and J. Pyun, *RSC Adv.*, 2015, **5**, 24718–24722.

89 J. J. Griebel, G. Li, R. S. Glass, K. Char and J. Pyun, *J. Polym. Sci., Part A: Polym. Chem.*, 2015, **53**, 173–177.

90 J. J. Griebel, N. A. Nguyen, S. Namnabat, L. E. Anderson, R. S. Glass, R. A. Norwood, M. E. MacKay, K. Char and J. Pyun, *ACS Macro Lett.*, 2015, **4**, 862–866.

91 V. P. Oleshko, J. Kim, J. L. Schaefer, S. D. Hudson, C. L. Soles, A. G. Simmonds, J. J. Griebel, R. S. Glass, K. Char and J. Pyun, *MRS Commun.*, 2015, **5**, 353–364.

92 J. J. Griebel, N. A. Nguyen, A. V. Astashkin, R. S. Glass, M. E. MacKay, K. Char and J. Pyun, *ACS Macro Lett.*, 2014, **3**, 1258–1261.

93 S. Namnabat, J. J. Gabriel, J. Pyun and R. A. Norwood, *Proc. SPIE*, 2014, **8983**, 89830D.

94 A. G. Simmonds, J. J. Griebel, J. Park, K. R. Kim, W. J. Chung, V. P. Oleshko, J. Kim, E. T. Kim, R. S. Glass, C. L. Soles, Y.-E. Sung, K. Char and J. Pyun, *ACS Macro Lett.*, 2014, **3**, 229–232.

95 M. Mann, E. Kruger Jessica, F. Andari, J. McErlean, R. Gascooke Jason, A. Smith Jessica, J. H. Worthington Max, C. C. McKinley Cheylan, A. Campbell Jonathan, A. Lewis David, T. Hasell, V. Perkins Michael and M. Chalker Justin, *Org. Biomol. Chem.*, 2019, **17**, 1929–1936.

96 T. Hasell, D. J. Parker, H. A. Jones, T. McAllister and S. M. Howdle, *Chem. Commun.*, 2016, **52**, 5383–5386.

97 C. Herrera, K. J. Ysinga and C. L. Jenkins, *ACS Appl. Mater. Interfaces*, 2019, **11**, 35312–35318.

98 J. A. Smith, X. Wu, N. G. Berry and T. Hasell, *J. Polym. Sci., Part A: Polym. Chem.*, 2018, **56**, 1777–1781.

99 C. B. Meyer, T. Stroyer-Hansen, D. Jensen and T. V. Oommen, *J. Am. Chem. Soc.*, 1971, **93**, 1034–1035.

100 B. Meyer, *Chem. Rev.*, 1964, **64**, 429–451.

101 J. J. Dale, S. Petcher and T. Hasell, *ACS Appl. Polym. Mater.*, 2022, **4**, 3169–3173.